

## **EMISSION SPECTRA OF LASER-INDUCED PLASMAS AT THE ELEMENTAL ANALYSIS OF SOLIDS: MEASUREMENT AND MODELING RESULTS**

E. Ershov-Pavlov<sup>1</sup>, K. Catsalap<sup>1</sup>, V. Rozantsev<sup>1</sup>,  
Yu. Stankevich<sup>2</sup>, K. Stepanov<sup>2</sup>

<sup>1</sup>*Institute of Molecular and Atomic Physics, Minsk, Belarus*

<sup>2</sup>*Heat and Mass Transfer Institute, Minsk, Belarus*

**Abstract.** Results are presented of measurements and numerical modeling of emission spectra of laser plasma plumes arising on surfaces of metal samples at their elemental analysis by the laser-induced breakdown spectroscopy (LIBS) technique. The plasma plumes have been considered, which are induced by single and double laser pulses of the nanosecond range duration.

The modeling of the plume plasma parameters consists of a solution of the thermal, hydro-dynamics and optical problems accounting for the laser beam action on a solid surface. The numerical code allows investigating the dynamics of two-dimensional erosion plumes supposing their axial symmetry. Resulting space and time distributions of parameters in the laser-induced plasmas are used to evaluate the plumes emission spectra supposing a side-on observation case.

The simulation results, which have been obtained for an Al-sample, are compared to the experimental ones, measured at the conditions of common LIBS applications: a Q-switched Nd:YAG laser generating pulses of 15 ns duration and 50 mJ energy at 1064 nm wavelength, which provided  $\sim 0.85 \cdot 10^9$  W/cm<sup>2</sup> maximum irradiance of the sample surface.

The comparative study is realized for the measured and simulated spectra of the plasma plumes induced at single- and double-pulse excitation modes, which allows examining reasons of the observed efficiency increase of the LIBS elemental analysis at the double-pulse excitation mode.

## 1. INTRODUCTION

The laser-induced breakdown spectroscopy (LIBS) is nowadays considered to be one of the most promising techniques of the elemental analysis of different types of materials including solids, liquids and gases (see, e.g., [1-3]). The main feature of the LIBS consists of the sample material ablation and excitation till plasma state by powerful pulse laser radiation. It results in the technique unique properties allowing to combine sampling and excitation in a single step and to make rapid in situ and, if necessary, distant analysis with no or minimum sample preparation. Additionally, by due focusing the laser beam one can control position and dimension of the laser erosion spot, as well as the ablation rate, which gives other advantages of the LIBS such as an opportunity of surface mapping and in-depth profiling of the sample elemental composition [4].

Unfortunately, common LIBS techniques have rather moderate sensitivity and measurement precision in comparison with the most developed spectroscopy techniques such as atomic absorption spectrometry (AAS) and inductively coupled plasma - atomic emission spectrometry (ICP-AES) [3], and efforts are being made to increase LIBS analytical efficiency. Among other ways, double-pulse laser excitation technique has been proposed, where the laser erosion plasma is produced by two laser pulses following each other with a certain delay compared to the plasma decay time. The double-pulse (DP) technique use and development as applied to the elemental analysis of solids in air began in 1980's [5-8]. Now a growing interest to the technique can be observed by publications, where different ways of the double-pulse technique realization are considered (see, e.g., [9-19]). Among them, one can find collinear [9-14] and orthogonal (pre-ablation [15-17] and reheating [18, 19]) schemes of the laser pulses (beams) action on samples of different compositions at various laser pulse parameters: energy, duration, wavelength, etc. All schemes give more or less apparent intensity increase of atomic and especially ionic lines in emission spectra of the DP laser plume as compared to one of a single pulse of the same total energy in the common single-pulse (SP) mode.

In spite of the technique active investigation, up to now there is no clear and complete understanding of the processes and mechanisms providing the observed phenomena of the line intensity increase. It is only clear, that the laser beams acting on a sample at the double-pulse mode produce a plasma volume having conditions (density, range and space-time distribution of the plasma parameters), which are more favorable for the emission of the lines under consideration [11, 12, 20, 21]. Further experiments including measurements of the laser plasma parameters with high time and space resolution will provide data for the problem solution. Together with the experiments, numerical modeling of the laser plumes would help much in the problem deeper understanding. One can find some interesting results concerning the laser plume simulation [22-25], but up to now there is actually no model providing an adequate account for the plume formation and expansion, as well as for the plume emission spectra. More, no models have been reported for the double-pulse laser plasma.

Here some results are presented of measurements and numerical simulation of line emission spectra of the laser plumes arising at both single- and double-pulse modes on Al-sample irradiated by a Q-switched Nd:YAG laser beam at the collinear illumination scheme. For this, data on distribution and evolution of plasma parameters in the laser plumes have been obtained first using a part of the numerical code reported earlier [21]. Resulting space and time distributions of the laser-induced plasma parameters have been used to evaluate the emission spectra of the plasma volumes at chosen time intervals supposing a side-on observation. The results have been compared to the experimental spectra measured in the conditions similar as close as possible to those considered at the simulation. The laser generated pulses of 15 ns duration and 50 mJ energy at 1064 nm, which provided  $\sim 0.8 \cdot 10^9$  W/cm<sup>2</sup> maximum irradiance of the sample surface. The aim of the work consists of comparative analysis of the simulation and measurement data on the laser plume formation, space-time behavior and resulting spectral emission of the plume at both action modes. The analysis results must help to clear up a difference in formation of the laser plumes arising at SP and DP modes, as well as of their emission spectra to finally understand reasons of the spectral line intensity increase at the double-pulse mode.

## 2. MODELING

The numerical code developed consists of two parts. The first one serves to evaluate the laser plumes formation, i.e. to find parameters of the laser-induced plasma, their instantaneous space distributions and the distributions evolution in time. The second one allows evaluating spectral emission of the laser plumes at a given distribution of the parameters along the observation line by solving the radiation transfer problem.

Laser plume formation modeling. The model considers a range of moderate ( $10^5$ - $10^{10}$  W/cm<sup>2</sup>) laser irradiation of a solid sample surface. The modeling of the plume plasma parameters supposes a self-consistent solution of the thermal, hydrodynamics and optical problems at the laser beam action on solids. The thermal problem accounts for the processes of heating, melting and evaporation of the samples. Dynamics of the solid samples heating and evaporation is described by a non-stationary heat transfer equation taking into account a dependence on temperature of the thermodynamic characteristics of the sample material

$$\frac{\partial(\rho_{\text{sol}} c_p T)}{\partial t} + \text{div } \vec{W} = 0; \quad \vec{W} = -\chi(T) \cdot \text{grad}T. \quad (1)$$

at the boundary conditions

$$\begin{aligned} W_z(r, z = 0, t) &= (1 - R)q(r, z = 0, t) - \rho_{\text{sol}} V_{\text{sub}} \Delta H, \\ V_{\text{sub}} &= \frac{\rho_{\text{vap}}(T_s) \sqrt{\gamma k T_s / m}}{\rho_{\text{sol}}}. \end{aligned} \quad (2)$$

where  $\rho_{\text{sol}}$  and  $\rho_{\text{vap}}$  are density of the sample and vapor, respectively,  $c_p$  – is specific heat,  $W$  and  $\chi$  are heat flux and heat conduction coefficient, respectively, at temperature  $T$ ,  $q$  is laser beam irradiance,  $\Delta H$  is evaporation specific enthalpy,  $V_{\text{sub}}$  is evaporation rate,  $\gamma$  is adiabatic index,  $R$  is a reflection coefficient of the laser radiation at the sample surface.

Gas-dynamics part of the code determines an expansion of the erosion products into the surrounding atmosphere, absorption of the laser radiation by the plume, as well as the resulting plasma evolution after the laser pulse is over. The dynamics of the laser plume expansion is accounted for by a system of the equations of mass, pulse and energy conservation, to which equations are added determining intensity of the laser emission incident to the sample surface and reflected from it:

$$\begin{aligned} \frac{\partial \rho}{\partial t} + \text{div}(\rho \vec{V}) &= 0 \\ \frac{\partial \rho u}{\partial t} + \text{div}(\rho u \vec{V}) + \frac{\partial P}{\partial z} &= 0 \\ \frac{\partial \rho v}{\partial t} + \text{div}(\rho v \vec{V}) + \frac{\partial P}{\partial r} &= 0 \\ \frac{\partial \rho E}{\partial t} + \text{div}((\rho E + P) \vec{V}) + \frac{\partial q_+}{\partial z} - \frac{\partial q_-}{\partial z} &= 0 \end{aligned} \quad (3)$$

Here  $u$  and  $v$  are, respectively, axial and radial components of the velocity vector  $\vec{V}$ ,  $P$  is pressure,  $E = \varepsilon + \vec{V}^2 / 2$  is total specific energy of the plasma with internal energy  $\varepsilon$ . The laser emission intensity directed to the surface  $q_-$  and reflected from it  $q_+$  is determined by the expressions

$$\begin{aligned} q_-(r, z, t) &= q(r, \infty, t) \cdot \exp\left(-\int_z^\infty \kappa_L dz'\right), \\ q_+(r, z, t) &= R(T_s) \cdot q_-(r, 0, t) \cdot \exp\left(-\int_0^z \kappa_L dz'\right), \end{aligned} \quad (4)$$

where  $\kappa_L$  is the plasma absorption coefficient at the laser wavelength, and  $R(T_s)$  is mentioned above the reflection coefficient of the laser radiation at the sample surface generally depending on temperature.

Boundary conditions taken into account at the problem solution can be written as follows:

$$\rho(r \leq r_{\text{spot}}) = \rho_{\text{vap}}(T_s); \quad P(r \leq r_{\text{spot}}) = P_{\text{vap}}(T_s); \quad u(r \leq r_{\text{spot}}) = \sqrt{\gamma k T_s / m}; \quad \varepsilon(r \leq r_{\text{spot}}) = \varepsilon(T_s). \quad (5)$$

The above system of equations is solved taken into account data of state equations and of absorption coefficient of the plasma under consideration, which are

pre-calculated supposing the plasma is in the local thermodynamic equilibrium and taken in a tabulated form:

$$T = T(\rho, \varepsilon); \quad P = P(\rho, \varepsilon); \quad N_e = N_e(\rho, \varepsilon); \quad \kappa_L = \kappa_L(T, \rho) \quad (6)$$

The plasma absorption coefficient at the laser emission frequency is calculated taking into account main mechanisms of the absorption in the plasma (bremsstrahlung, photoionization and selective absorption). Thermal radiation transfer in the laser plume, as well as a difference in thermo-dynamical and optical properties of the erosion products and of ambient air are not taken into account at the calculations.

The code allows evaluating the dynamics of two-dimensional erosion plumes supposing their axial symmetry accounted for by  $r$ - and  $z$ -coordinates. A distribution of the power density across the laser spot on a sample surface is set to be Gaussian and to depend only on the radial coordinate  $r$ . The laser beam is supposed to have a cylindrical form and to fall normally on the sample surface. A dependence of the laser power density on time can be fitted to real experimental data. The calculation results are 2D distributions of the erosion plasma temperature, density and pressure depending on time after the laser beam incidence. More detail on the modeling code can be found in [26].

Line spectra modeling of the laser plume. Space-time characteristics of the laser erosion plasma, which are obtained at the plasma formation modeling discussed above, serve as initial data for the emission spectra simulation. From the data, one finds distributions  $T(x)$ ,  $\rho(x)$  of the plasma temperature and density along an observation line  $x$  and a time moment chosen. For every point of the distributions at given  $T(x)$ ,  $\rho(x)$ , one determines the plasma elemental composition

$$\rho = m_H \sum_k \beta_k A_k \sum_{i=1}^{Z_k+1} N_{ki}, \quad (7)$$

where  $\rho$  is plasma density in  $\text{g/cm}^3$ ,  $m_H = 1.66 \cdot 10^{-24}$  g is mass of hydrogen atom,  $k$  designates different chemical elements in the plasma. Every element has  $\beta_k$  volume ratio,  $A_k$  atomic number and  $N_{ki}$  ( $\text{cm}^{-3}$ ) number density of atoms and ions ( $N_{k1}$  for neutral,  $N_{k2}$  for the first ion, etc.).

Further, the plasma ionization composition and population density of excited states are found using equations of the ionization equilibrium for every element in the sample [27]:

$$\frac{N_{i+1}N_e}{N_i} = 2 \left( \frac{2\pi mkT}{h^2} \right)^{3/2} \frac{U_{i+1}}{U_i} \exp[-(J_i - \Delta J_i)/kT], \quad (8)$$

Partition functions of atoms and ions are calculated according to Planck – Larkin approximation:

$$U_i = \sum_j g_{ij} \exp(-E_{ij}/kT) W_{ij}, \quad W_{ij} = 1 - \left( 1 + \frac{J_i - E_{ij}}{kT} \right) \exp\left( \frac{E_{ij} - J_i}{kT} \right). \quad (9)$$

Here  $U_i$  is partition function of ions of the  $i$ -th ionization degree,  $g_{ij}$  and  $E_{ij}$  are their statistical weight and energy of the  $j$ -th level, respectively,  $W_{ij}$  is Planck – Larkin factor.

The ionization potential lowering  $\Delta J_i$  due to Coulomb interaction of particles can be written as follows:

$$\Delta J_i = kT \ln \frac{(1 + \gamma/2) \left[ 1 + (z_i + 1)^2 \gamma/2 \right]}{(1 + z_i^2 \gamma/2)}, \quad (10)$$

where  $z_i$  is charge of ion ( $i=1$  for neutral atom),  $\gamma$  is determined as a positive route of the equation

$$\gamma^2 = \left( \frac{e^2}{kT} \right)^3 4\pi \sum_i \frac{n_i z_i^2}{1 + z_i^2 \gamma/2}, \quad (11)$$

and for weakly non-ideal plasma it coincides with the common non-ideality parameter.

For the calculation of the particles partition functions, a database is incorporated in the program on energy levels and statistical weights of atoms and ions of different chemical elements.

Further in the program, spectral emission  $j_\lambda$  and absorption  $\kappa_\lambda$  coefficients are calculated for chosen lines in radiation spectra of the laser plumes under consideration

$$j_\lambda = A_{mn} \frac{hc}{\lambda_0} N_m \phi(\lambda) = \kappa_\lambda 4\pi I_{\lambda p}.$$

$$\kappa_\lambda = \frac{\pi e^2 \lambda_0^2}{mc^2} f_{nm} N_n \left[ 1 - \exp\left( -\frac{hc}{\lambda_0 kT} \right) \right] \phi(\lambda), \quad (12)$$

where  $A_{mn}$  and  $f_{nm}$  are, respectively, transition probability and oscillator strength for the line optical transition,  $I_{\lambda P}$  is spectral intensity of the black body radiation,  $\phi(\lambda)$  is spectral profile of the plasma emission coefficient within the line. Stark broadening is considered in the program as the main mechanism forming line profiles in the laser plume emission spectra. In this case, emission coefficients for the lines have Lorentzian profiles and can be accounted for by the expression [28]

$$\phi(\lambda) = (\gamma_e / \pi) [\gamma_e^2 + (\lambda - \lambda_0 - \delta_e)^2]^{-1}, \quad (13)$$

where  $\gamma_e$  and  $\delta_e$  are half-width and shift, respectively, of the profile. These profile parameters are taken proportional to the electron density

$$\gamma_e = w(T) \cdot N_e \cdot 10^{-16}, \quad \delta_e = d(T) \cdot N_e \cdot 10^{-16}. \quad (14)$$

The proportionality coefficients  $w(T)$  and  $d(T)$  are known as Stark broadening parameters for the width and shift, respectively. At this approximation, no possible influence of ion micro-fields is taken into account.

Spectral line intensity in the laser plume emission is determined by numerical solution of the radiation transfer equation [29]

$$I_\lambda(\tau) = I_\lambda(0) \exp(-\tau) + \int_0^\tau I_{\lambda P}(\tau') \exp(\tau' - \tau) d\tau',$$

$$\tau = \int_y^{r_0} \kappa_\lambda(y') dy', \quad (15)$$

where  $r_0$  is the plume radial border at a given time moment. The equation solution procedure and spectral line intensity evaluation is performed similar to [30].

The numerical solution of (15) is reduced to a recursion relation for the intensities of the radiation at the neighboring space points [31]. The plasma parameters (ionization state, spectral emission, absorption coefficient and their profiles for the selected line) are calculated at chosen discrete points on the observation line taken into account the temperature profile obtained at the plasma plume formation modeling. Parameters of the optical transitions resulting in the emission of chosen spectral lines, including the lines Stark broadening parameters, transition probabilities and statistical weights of the energy levels, are taken from [28, 32].

### 3. EXPERIMENTAL

Experimental measurements have been performed using a Laser Spectrochemical Analyzer (LSA) [20]. A general view of LSA and its schematic diagram are shown in Fig. 1. LSA is composed of a

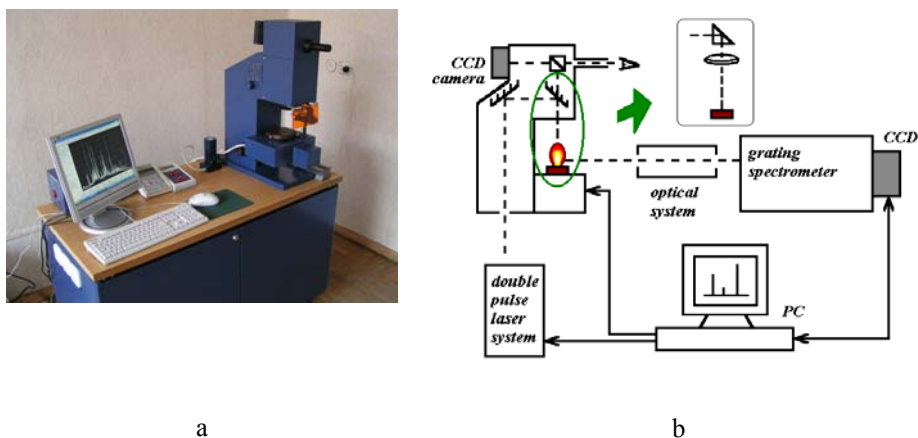


**Fig. 1.** Laser spectrochemical analyzer: (a) general view and (b) schematic diagram.

Q-switched Nd:YAG double pulse laser, an optical unit consisting of microscope, imaging CCD-camera and PC-controlled sample table, a spectrometer with a CCD-arrays recording system. The laser works at wavelength of 1064 nm. The laser pulses duration and frequency can be controlled in the intervals of 10-20 ns and 1-15 Hz, respectively. The pulses energy is also variable and can be set as high as 100 mJ. The laser can work both in the single- and double-pulse modes at the collinear scheme of the laser beams action on a sample. A time delay between the pulses can be regulated from 0 to 140  $\mu$ s. The laser action zone is imaged at the PC monitor and can be positioned on a sample with 0.01 mm accuracy. LSA is equipped with a 1-meter grating spectrometer for recording the spectral emission of the laser plumes. Wavelength working interval and spectral resolution of the spectrometer are 200 – 800 nm and 20000, respectively. An optical system serves to deliver the plasma plume emission to the spectrometer entrance slit. LSA operates at a PC control. The PC software allows recording and treatment the plume emission spectra and the erosion crater images, as well as plotting calibration graphs and evaluating elemental compositions of samples.

#### 4. RESULTS AND DISCUSSION

A study has been performed of formation and space-time evolution of laser ablation plumes on aluminum sample in atmospheric pressure air at single- and double-pulse excitation modes. The plume emission spectra have been recorded in the spectral interval of 250-400 nm at 0.74 nm/mm dispersion and 0.015 nm spectral resolution using LSA equipped with PGS-2 spectrograph and TCD1205 CCD array. A side-on observation has been chosen for the measurements. The optical axis has been directed along the sample surface at a chosen distance  $z$  from it. The plumes have been imaged 3:1 by lenses onto an intermediate slit (diaphragm). The slit edges are perpendicular to the plume axis discriminating a part of the plume of 1 mm height. The second optical system after the diaphragm collected total emission of the “disk” to the spectrograph entrance slit. Displacing the diaphragm along the plume axis, one could record the plume emission at different distances  $z$  from the surface. The measurements spatial resolution was estimated to be 0.1 and 0.5 mm along the axial and radial directions, respectively.

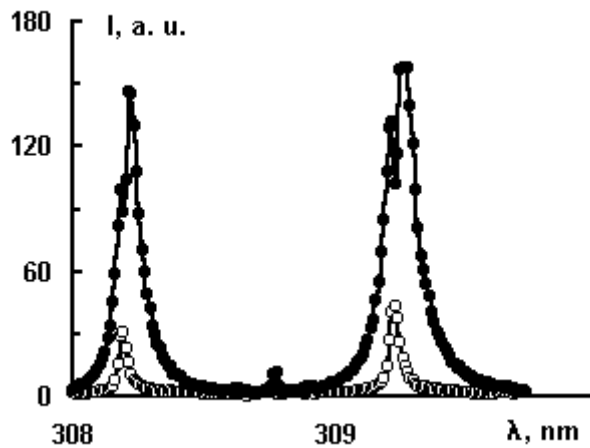


**Fig. 2.** Emission spectra of the laser-induced Al plasma at SP (open circles) and DP (solid circles) modes recorded 1 mm above the sample surface (one can see atomic lines Al I 308.2 and Al I 309.3 nm).

The measurements have been performed at the action on Al sample polished surface of the laser pulses of 0.05 J energy and 15 ns (FWHM) duration with a “tail” up to 75 ns. The laser beam was focused 5 mm below the surface. For one single-pulse shot, it resulted in 820 MW/cm<sup>2</sup> maximum irradiation of the sample surface at a near-Gaussian spatial distribution with 0.54 mm characteristic radius. At the spectra recording, the sample was irradiated with a series of single or double pulses at 10 Hz frequency. Total emission of laser plumes from 80 single pulses and

40 double pulses at SP and DP modes, respectively, was recorded to increase the signal level keeping equal energy at both modes. The signal measurements were performed with no time resolution. The sample was not moved during the spectra recording. A time delay of 5  $\mu\text{s}$  was realized between the first and the second pulses at the DP mode. The delay was shown to give the most pronounced effect of the DP mode at the conditions under consideration [20]. The intensity increase at DP mode for this work conditions is demonstrated by Fig. 2, where recorded at the both modes spectra of the laser plume emission in a spectral region of Al I atomic lines are presented.

The numerical modeling has been performed at the same conditions as the measurements. The reflection coefficient of the sample  $R=0.9$  has been taken and accepted to be constant. At the simulation of the laser plume formation at DP mode, conditions and plasma parameters of the first laser pulse plume formed to the moment equal to a given time delay between the pulses have been taken as initial ones for the space-time characteristics calculation of the laser plume induced by the second laser pulse. For the rest, the calculation procedure has been performed analogous to the SP plume simulation.

According to the modeling results for the SP mode, the evaporation begins at 8 ns, at 15 ns the plasma occurs, at 30 ns the ablation plume shields the sample preventing material erosion. Further, the laser radiation is totally absorbed by the ablation plume, and a wave of absorption propagates towards the laser beam in the light detonation regime. When the laser pulse is over, the wave of absorption is at 0.5 mm distance from the sample surface, and the plume expansion still has a “one-dimensional” character. Radial inhomogeneity of the laser plume is determined by the distribution of the power density over the erosion spot.

The main difference of the second pulse action at DP mode is existence of a sheet of strongly absorbing plasma near the sample surface. The plasma optical density is around  $5 \cdot 10^{-3}$  to the moment of the second pulse action. The density reaches 1 already in 20 ns and 3 in 22 ns after the second pulse begins. The latter value is characteristic for the main time interval of the laser pulse action. The optical density slow decrease begins only in 60 ns from the pulse beginning. Thus according to the calculation, the sample surface is actually shielded from the laser radiation. The radiation strong absorption by plasma results in an increase of the plume dimension in both radial and axial directions. One can observe the increase in Fig. 3, where axial distributions of plasma temperature and density in a laser pulse at SP and in the second pulse at DP modes are shown for different moments from the due pulse action.

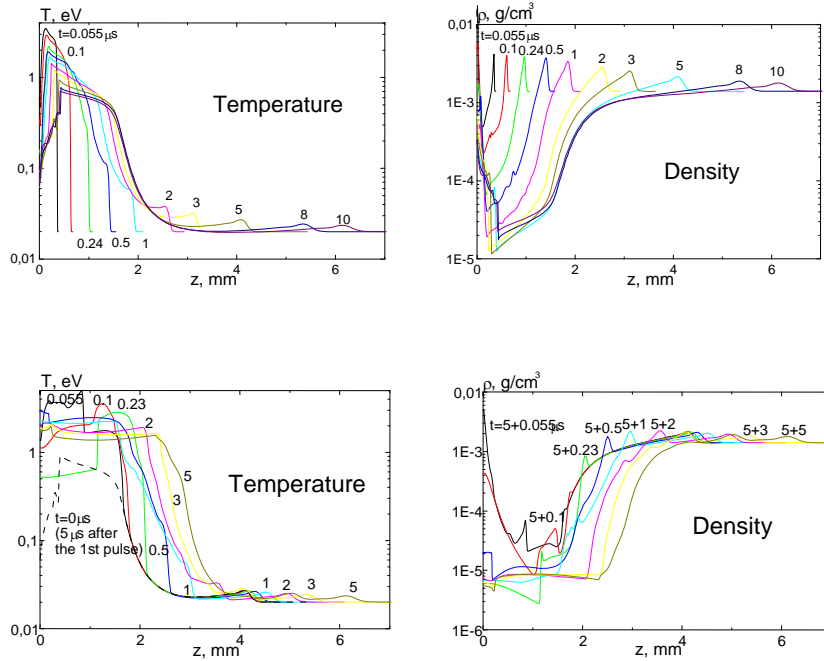


**Fig. 3.** Axial distribution of plasma temperature and density in the laser plumes at SP (up) and DP (down) modes at different time intervals from the laser pulse action (shown in micro-seconds).

Time evolution of radial distributions of plasma temperature and density in the SP and DP laser plumes is demonstrated by Fig. 4, where the distributions at  $z=1$  mm for different time intervals from the laser pulse action (the second one for the DP mode) are shown. Comparing to the SP plume, higher temperature (20-30 kK, instead of 5-10 kK) and lower density are characteristic for central parts of the DP laser plume. Also the DP plume has complex non-monotonous temperature profiles, contrary to those at the SP mode having one central maximum and nearly parabolic shape. For the first 1-2  $\mu$ s, pressure is higher in the SP plume, but further it is close to the ambient (atmospheric) one in the both modes.

The radial distributions have been used for the calculations of “side-on recorded” intensity of the spectral line chosen. They have been mostly limited with the temperature of 3000 K. At lower temperature, density of excited atoms is too low and their emission can be neglected. Also, Al vapor condensation begins in this temperature region. Spectral line intensities for all time moments considered have been integrated to obtain the value corresponding to the experimental one measured without any resolution in time.

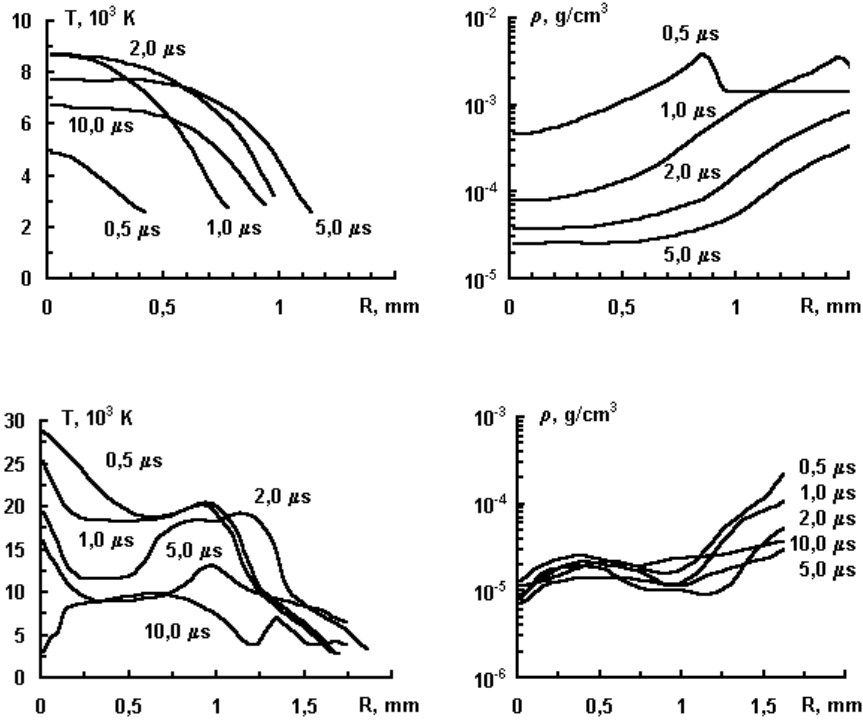


**Fig. 4.** Radial profiles of temperature (left) and density (right) in the laser plumes at the SP (up) and DP (down) modes for a distance  $z=1$  mm from the sample surface at different time intervals from the laser pulse action (shown in micro-seconds).

An example of the results is presented in Fig. 5, where measured and numerically simulated spectral profiles are presented for integrated in time intensity of Al II line at  $\lambda=281.6$  nm in emission of the laser plumes at the SP and DP modes at  $z=1$  mm. As far as no absolute calibration has been performed of the experimental data, they were reduced to the absolute scale of the values obtained at the simulation by equalization maxima of the measured and calculated DP line profiles. It is seen that the ion line SP intensity is close to a detection limit and the DP intensity is more than 10 times higher. One can observe a fair agreement of the measured and simulated DP line profiles.

Generally, it is observed that the intensity increase in DP spectra compared to SP ones depends on excitation energy of the lines under consideration. It increases with the excitation energy and it is much stronger for ion than for atomic lines (see, e.g., [20, 33, 34]). This difference is more pronounced for the integrated

in time emission intensity of laser plumes. The observation is confirmed also by the data of our measurements exposed in figures 2 and 5.

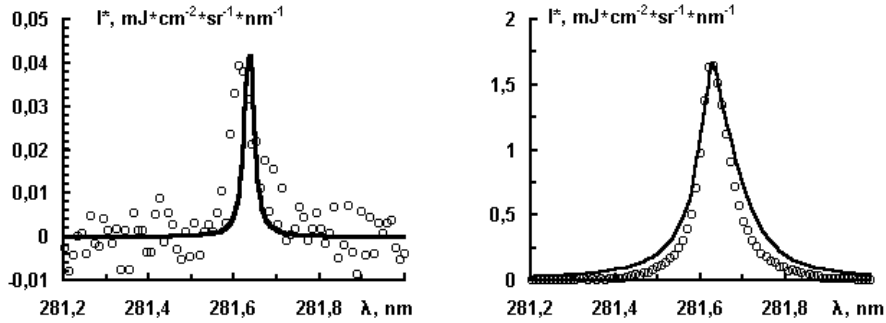


**Fig. 5.** Measured (points) and simulated (lines) profiles of Al II 281.6 nm line in the laser plume emission at SP (left) and DP (right) modes for a side on observation at  $z=1$  mm from the sample surface.

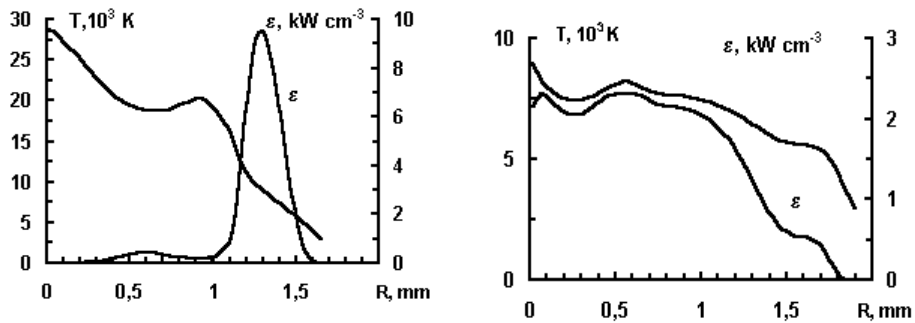


**Fig. 6.** Radial distribution of plasma temperature and emission coefficient for atomic Al I 308.2 nm line in the DP laser plume and  $z=1$  mm at 0.5 (left) and 15 (right)  $\mu\text{s}$  from the second pulse action.

Our numerical simulation data allow better understanding reasons of the intensity increase at DP mode and its dependence on excitation energy of spectral lines. In Fig. 6, radial distributions are shown of plasma temperature and emission coefficient for atomic Al I 308.2 nm line in the DP laser plume at 0.5 and 15  $\mu\text{s}$  from the second pulse action. One can see from the figure that at initial time

moments the atomic line intensity in the laser plume emission spectrum is provided by a narrow space zone at the plume periphery, where the line emission coefficient is high. It is due to a relatively low (around 8000 K) “normal temperature” [35] of the line and to a rather steep temperature radial gradient. In this case, the DP line intensity can be not very different from the intensity at the SP mode, where the plasma temperature does not prevail “normal” one (see Fig. 4). On the contrary, later when the plasma temperature decreases, a zone of the line effective emission occupies nearly all plasma plume volume on the observation line, and the line intensity can noticeably grow up in comparison with the SP mode. The intensity increase will depend on the effective volume dimension. For ion lines the effective emission volume at the DP mode will be much larger from the beginning of the plume expansion. Additionally, the ion emission coefficient will rise strongly over the plume volume due to the elevated “normal temperature”, which in most zones is much higher than the DP plasma temperature resulting in the steep coefficient dependence on temperature.

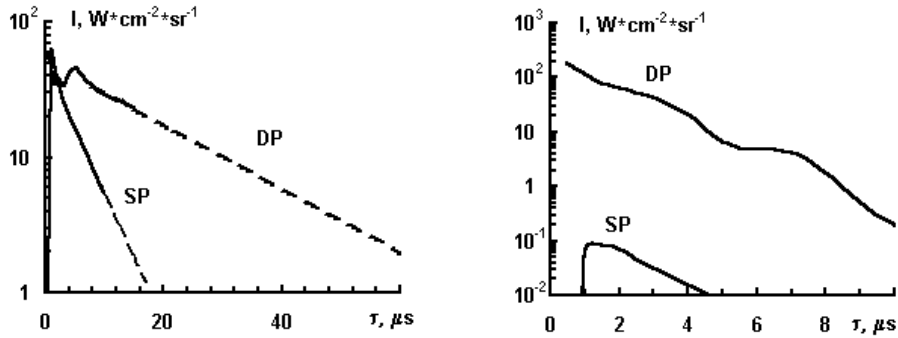


**Fig. 7.** Total intensity of atomic Al I 308.2 nm (left) and ionic Al II 281.6 nm (right) spectral lines in the SP and DP laser plume emission at  $z=1$  mm depending on time from the laser pulse action. Dashed line shows the data extrapolation.

A behavior in time of the lines intensity in emission spectra of the plumes can be analyzed using Fig. 7, where total intensity of atomic Al I 308.2 nm and ionic Al II 281.6 nm spectral lines in the SP and DP laser plume emission is presented depending on time from the laser pulse action. It is seen from the figure that the DP intensity increase of the atomic line depends on time from the laser pulse action, and for small time intervals one can find no efficiency increase of the DP mode. Possibly, it can explain controversial evaluations of the DP mode influence on atomic line intensity, which can be observed in some papers.

Generally, one can see that for the DP laser plume higher plasma temperature, the plume volume and duration are characteristic. All the factors play certain roles in the observed increase of line intensity in DP plume emission spectra. The factors influence on atomic and ionic lines can be different depending on a temperature interval realized. In our case, the DP intensity amplification of atomic

lines is mainly due to an increase of the effective emission volume dimension and duration. As for the DP intensity of ionic lines, its growth is provided more by the temperature (emission coefficient) increase.

The numerical simulation results on the line intensity in the total emission spectra of SP and DP plumes have been compared to our experimental data. According to the measurement mode, total intensity of atomic Al I 308.2 nm and ionic Al II 281.6 nm lines in emission spectra of the plumes observed at different distances  $z$  from the sample surface have been calculated. For every  $z$ , the intensity has been integrated over all life time of the plumes. The emission intensity of both pulses at the DP mode has been summed and doubled SP intensity has been taken to compare to each other and to analogous measured values. The measured intensity has been reduced to the calculated intensity scale supposing the intensity values of the SP emission obtained at the simulation and measurements at  $z=0.5$  mm are equal. The results obtained are shown in Fig. 8.

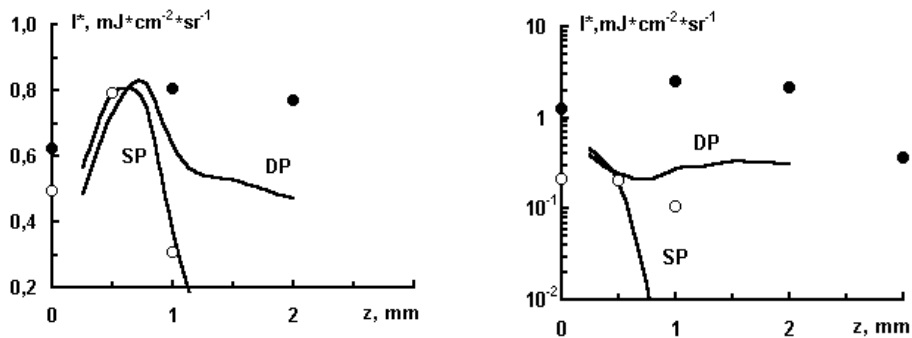


**Fig. 8.** Integrated in time intensity of atomic Al I 308.2 nm (left) and ionic Al II 281.6 nm (right) lines in emission spectra of the laser plume depending on distance  $z$  from the sample surface: lines present the modeling results, points show the measurements data for the SP (open circles) and DP (solid circles) modes.

From the figure it follows that the DP plumes are larger than SP ones and the DP intensity gain depends on a distance  $z$  from the sample of the side-on observation line. The gain increases with the distance from the sample. One can state a rather fair agreement of the experiment and simulation data at the SP mode, especially for the atomic line. (Note, the measured values at  $z=0$  can be distorted by the sample border shielding). Generally, experimentally observed plumes are larger than the simulated ones. Partly it can be explained by the radiation energy transfer in the plumes, which is not taken into account in the modeling code. Also, laser erosion of the sample can be higher, than it is given by the model, where constant reflection coefficient is used for both laser plumes in the DP mode.

## 5. CONCLUSION

Numerical simulation and measurements have been performed of the intensity of atomic and ionic lines in emission spectra at a side-on observation of erosion plasma induced by pulses of a Q-switched Nd:YAG laser on Al sample in single and double pulse excitation modes for typical LIBS conditions. The spectra have been obtained by a numerical solution of the radiation transfer equation for radial distributions of the erosion plasma parameters, taken from the laser plume numerical modeling. The modeling consists of a solution the thermal, hydro-dynamics and optical problems accounting for the laser beam action on a solid surface. The numerical code allows a simulation of the dynamics of two-dimensional erosion plumes supposing their axial symmetry.

A qualitative correlation of the calculated and measured data is observed. The comparison seems to show an important role of the radiation transfer processes in the laser plume formation. The DP plasma expansion lasts longer and it occupies larger volume with non-monotonous temperature distributions. Also, an increase of the laser plasma temperature is observed at the DP mode.

These changes result in the observed increase of line intensity in the DP plume emission spectra. The intensity gain is due to the emitting plasma temperature and volume increase. A role of the factors is different for atomic and ionic lines. In our case, when the DP plasma temperature overcome “normal temperature” for atomic lines, their emission is formed mainly in the plume periphery, and the main reason for their intensity increase is mainly the plasma volume and duration increase. The ionic line intensity increases mainly due to higher plasma temperature (emission coefficient). Note, sometimes one finds no increase in DP plasma temperature measured by relative intensity of atomic lines. It can be shown that such measurement for the considered inhomogeneous laser plasma must give rather a temperature value close to “normal temperatures” of the atomic line used [36].

Further, it is supposed to consider more factors influencing sample erosion, especially at the DP mode and to develop the numerical code including calculations of the energy transfer by the laser plume own radiation with a detailed account of its angular and spectral characteristics.

## REFERENCES

1. L.J. Radziemski, *Spectrochim. Acta, Part B* **57**, 1109-1113 (2002).
2. N. Omenetto, *J. Anal. At. Spectrom.* **13**, 385-399 (1998).
3. J.D. Winefordner, I.B. Gornushkin, T. Correll et al., *J. Anal. At. Spectrom.* **19**, 1061-1083 (2004).
4. J.M. Vadillo, J.J. Laserna, *Spectrochim. Acta, Part B* **59**, 147-161 (2004).
5. V.A. Rozantsev, *Proc, Rep. Sci. Sem. Atom. Spectr. Analys. Minsk*, 12-14 (1978).
6. V.A. Rozantsev, V.A. Kononov, VII Rep. Conf. Young Sci. on Phys. Abstracts, Mogiliov, 123 (1982).
7. S.M. Pershin, *Quantum Electronics*, **16**, 325-330 (1982).

8. K. Takaharu, S. Hiroya, S. Koichi, M. Katsusuke, Japanese Patent, JP62-85847 (1987).
9. V.A. Rozantsev, A.D. Shirokanov, A.A. Yankovsky, *Zhurn. Prikl. Spektrosk. (Rus)* **59**, 431-434 (1993).
10. L. St-Onge, V. Detalle, M. Sabsabi, *Spectrochim. Acta, Part B* **57**, 121-135 (2002).
11. R. Noll, R. Sattman, V. Sturm, S. Winkelmann, *J. Anal. At. Spectrom.* **19**, 419-428 (2004).
12. M. Corsi, G. Cristoforetti, M. Giuffrida, M. Hidalgo, S. Legnaioli, V. Palleschi, A. Salvetti, E. Tognoni, C. Vallebona, *Spectrochim. Acta, Part B* **59**, 723-735 (2004).
13. J.A. Aguilera, C. Aragon, *Spectrochim. Acta, Part B* **59**, 1861-1876 (2004).
14. X. Mao, X. Zeng, S.-B. Wen, R.E. Russo, *Spectrochim. Acta, Part B* **60**, 960-967 (2005).
15. D.N. Stratis, K.L. Eland, S.M. Angel, *Appl. Spectrosc.* **55**, 1297-1303 (2001).
16. C. Gautier, P. Fichet, D. Menut, J.-L. Lacour, D. L'Hermit, J. Dubessy, *Spectrochim. Acta, Part B* **60**, 265-276 (2005).
17. G. Cristoforetti, S. Legnaioli, L. Pardini, V. Palleschi, A. Salvetti, E. Tognoni, *Spectrochim. Acta, Part B* **61**, 340-350 (2006).
18. J. Uebbing, J. Brust, W. Sdorra, F. Leis, K. Niemax, *Appl. Spectrosc.* **45**, 1419-1423 (1991).
19. C. Gautier, P. Fichet, D. Menut, J.-L. Lacour, D. L'Hermit, J. Dubessy, *Spectrochim. Acta, Part B* **59**, 975-986 (2004).
20. E. Ershov-Pavlov, M. Petukh, V. Rozantsev, 2<sup>nd</sup> Euro-Mediter. Symp. on LIBS (Book of abstracts), Hersonissos, Crete, Greece, 12 (2003).
21. E. Ershov-Pavlov, Yu. Stankevich, and K. Stepanov, 3<sup>rd</sup> Euro-Mediter. Symp. on LIBS (EMSLIBS 2005), Aachen, Germany CD, 4-6\_AB10063 (2005).
22. I.B. Gornushkin, C.L. Stevenson, B.W. Smith, N. Omenetto, J.D. Winefordner, *Spectrochim. Acta, Part B* **56**, 1769-1785 (2001).
23. V.I. Mazhukin, V.V. Nossov, G. Flamant, I. Smurov, *J. Quant. Spectr. Rad. Transf.* **73**, 451-460 (2002).
24. A. Bogaerts, Z. Chen, R. Gijbels, A. Vertes, *Spectrochim. Acta, Part B* **58**, 1867-1893 (2003).
25. M. Capitelli, A. Casavola, G. Colonna, A. De Giacomo, *Spectrochim. Acta, Part B* **59**, 271-289 (2004).
26. G.S. Romanov, A.S. Smetannikov, Y.A. Stankevich, L.K. Stanchits, K.L. Stepanov, V Minsk Int. Heat & Mass Transfer Forum. Minsk, Proc. on CD, No 2.43 (2004).
27. G.S. Romanov, Yu.A. Stankevich, L.K. Stanchits, K.L. Stepanov, *Int. J. Heat and Mass Transfer* **38**, 545-556 (1995).
28. H.R. Griem, *Spectral Line Broadening by Plasmas*, N.-Y., London, Acad. Press, 1974.
29. E. A. Ershov-Pavlov and K. L. Stepanov, *J. Appl. Spectrosc.* **68**, 350-358 (2001).
30. E. A. Ershov-Pavlov, K.Yu. Katsalap, K. L. Stepanov, *J. Appl. Spectrosc.* **72**, 434-442 (2005).

31. E. A. Ershov-Pavlov, V. E. Okunev, Yu. A. Stankevich, L. K. Stanchits, K. L. Stepanov, *Publ. Obs. Astron. Belgrade* **66**, 19–33 (1999).
32. <http://www.nist.gov>
33. M.P. Petukh, V.A. Rozantsev, A.D. Shirokanov, A.A. Yankovsky, *Zhurn. Prikl. Spektrosk. (Rus)* **67**, 798-801 (2000).
34. C. Gautier, P. Fichet, D. Menut, J.-L. Lacour, D. L'Hermit, J. Dubessy, *Spectrochim. Acta, Part B* **60**, 792-804 (2005).
35. J.Richter, in *Plasma Diagnostics*, W. Lochte-Holtgreven ed., Amsterdam (1968).
36. E.A. Ershov-Pavlov, K.L. Stepanov, *Proc. 15<sup>th</sup> Int. Symp. Plasma Chem. (ISPC-15)*, Orleans. 3 1057-1062 (2001).